Proc. Estonian Acad. Sci. Phys. Math., 2004, **53**, 4, 252–265

Antarctic Circumpolar Current as a density-driven flow

Jaak Heinloo and Aleksander Toompuu

Marine Systems Institute at Tallinn University of Technology, Akadeemia tee 21, 12618 Tallinn, Estonia; heinloo@phys.sea.ee

Received 29 December 2003, in revised form 13 September 2004

Abstract. The paper considers the Antarctic Circumpolar Current (ACC) as a current formed due to the specific density field in the Southern Ocean characterized by relatively strong frontal zones. Unlike the approach founded on the geostrophic balance only, the suggested model takes into account turbulence effects caused by the baroclinic instability. The approach is grounded on the theory of rotationally anisotropic turbulence (RAT theory). While classical treatments of the ACC are based on the momentum balance, the RAT theory is founded on a simultaneous consideration of the momentum and moment of momentum balance. The equation of the moment of momentum is introduced due to the rotational anisotropy of turbulence in frontal region(s) coinciding with the observed ACC occurrence. For the realistic density field, estimated from the measured and optimally analysed temperature and salinity long-term data in the Southern Ocean with the density increasing to the south, the resulting velocity is directed to the east. This velocity is interpreted as the turbulence-generated ageostrophic constituent of the flow field. In the regions where turbulence effects are missing, the ageostrophic velocity constituent vanishes and the model reduces to the classical geostrophic balance condition. The model predictions are illustrated by velocity profiles calculated for the case where turbulent effects prevail over the geostrophic balance.

Key words: Southern Ocean, Antarctic Circumpolar Current, turbulence, zonal flow.

1. INTRODUCTION

The Antarctic Circumpolar Current (ACC) is the dominant flow in the Southern Ocean, meandering between about 50°S and 60°S and encircling the Antarctic continent in a clockwise direction as the motion is looked at from the South Pole. The current is characterized as consisting in general of several relatively narrow quasi-stationary branches coinciding with frontal regions of density [1–4]. Some branches of the ACC extend to considerable depths. The integral volume transport of the ACC, estimated from the data measured in the

Drake Passage as well as in the area between the Falkland Islands and South Georgia, is around 1.0–1.5 × 10^8 m^3 s^{-1} [1,2,5,6].

The common understanding of the ACC ties the current forcing with westerlies dominating in the region. Two different types of the ACC wind-driven models have been formulated. The first stems from the classical work of Munk and Palmén [7] and proceeds from the momentum balance with the momentum transfer by shear from surface to bottom, often complemented by the meridional overturning [8–11]. The second approach [12–14], started by Wyrtki [15], is based on the Sverdrup balance. Both approaches meet considerable difficulties.

The difficulties facing the wind-driven models [16], as well as the ongoing discussion [17–20] of the problem, prove that the very physical background of the ACC formation is still unclear and more effort is needed to understand it better. One of the unsolved problems is connected with the role of the density field in the formation of the ACC. Although the ACC (as well as its different branches) evidently coincides with the frontal zones of the density, the importance of the density field properties in the ACC formation has been left almost entirely out of the vision of the ACC wind-driven models.

The geostrophic balance would be the simplest explanation of the water density increase to the south in the ocean interior, accompanied by the ocean surface sloping up to the north. The slope, together with the varying density field, causes the pressure gradient to be directed to the north in the ocean interior down to the isopotential no-motion level. If the geostrophic balance condition holds, it determines the eastward flow above the no-motion level, which can be interpreted as the ACC. The geostrophic balance assumption is straightforward if the meridional density gradients are small. The conditions would change substantially for the density gradients sufficiently large to generate baroclinic instability. The instability generates turbulence fed by the potential energy stored in the frontal regions. Then the geostrophic balance would not hold in the region of turbulence occurrence and turbulence effects should be accounted for in the ACC models.

This paper discusses the turbulence-affected formation of the ACC. The turbulence is described by the theory of rotationally anisotropic turbulence (RAT) [21–23]. The discussion involves the model situation, where the effects of momentum, heat, and fresh water fluxes across the upper boundary are excluded, the vertical pressure gradient is balanced by the gravity force, and the density field is baroclinically unstable. The model assumptions lead to the vertical component of the force field emerging due to the generated turbulence rotational anisotropy balanced by the vertical component of the Coriolis force. This balance condition predicts an equilibrium zonal velocity constituent in frontal density regions. It vanishes if the turbulence effects are absent and can be interpreted as an ageostrophic turbulence-generated constituent of the total velocity field. For the turbulence effects dominating over the other effects influencing the flow formation, the model predicts a zonal flow (ACC) due to the turbulent processes only. For the absence of turbulence effects, the formulated model reduces to the classical geostrophic ACC model. The possibility of the ACC being founded on

turbulent processes only links the suggested ACC formation mechanism to the dynamics of atmospheres of fast rotating giant planets, the emerging zonal flows of which have also been considered as a result of turbulent processes [24,25].

The velocity calculations proceeding from the density field data in the Southern Ocean (Section 3) are presented in Section 4. It is shown that a particular model situation explaining the ACC by turbulent processes only is able to describe the main quality of the ACC (Section 4). Beside the most significant eastward zonal flow (ACC) in the Antarctic Convergence Zone (AC), extending to more than 3000 m depth and corresponding to the ACC, two other flow constituents were detected. An eastward flow occurs to the north of the modelled ACC and goes down to about 250 m depth, the other flow runs westward along the coastal shelf edge in the south. All three modelled current constituents have their counterparts from observations [3,26–28].

Section 5 treats the model situation calculated in Section 4 in terms of mass and energy balance. According to this treatment, all energetic processes forming the flow take place on the turbulent level of motion fed by the medium potential energy released due to baroclinic instability.

2. THE MODEL

2.1. The model set-up

Let us consider the motion between the surface and bottom boundary layers, with the stationary average velocity field $\boldsymbol{u}$ directed along longitude,

$$\boldsymbol{u} = (u(\vartheta, z), 0, 0). \tag{1}$$

In (1) and henceforth, the spherical co-ordinate system (φ, ϑ, z), where φ is longitude, ϑ is south latitude, and z is depth $(z \geq 0)$, is used. The ocean surface level is determined relative to the level $z = 0$ as $\xi = \xi(\vartheta) \geq 0$ $(\xi_{,\vartheta} \geq 0)$. Let us first assume $\xi = 0$; then all effects associated with the ocean surface slope will be excluded and only turbulence will drive the model. Accepting for potential density ρ (henceforth – the density) that $\rho = \rho_0 + \tilde{\rho}$, in which $\rho_0(0) = 10^3$ kg m^{-3}, $\tilde{\rho} << \rho_0$, applying the Boussinesq approximation [29], and neglecting the momentum transport due to the diffusivity (described by the symmetric constituent of the stress tensor), we simplify the momentum equation of the RAT theory [21–23] to the balance condition

$$-\nabla p + \frac{1}{2}\nabla \times \sigma + 2\rho_0 \boldsymbol{u} \times \omega^0 + \rho \boldsymbol{g} = 0. \tag{2}$$

In (2), p denotes pressure, ω^0 is angular velocity of the Earth's rotation, $\boldsymbol{g}$ is gravity acceleration, and

$$\sigma = 4\gamma(\Omega - \omega) \tag{3}$$

is the dual vector of the antisymmetric constituent of the stress tensor. In (3), Ω is defined as $\Omega = \left\langle \boldsymbol{v}' \times \boldsymbol{R} / R^2 \right\rangle$, where $\boldsymbol{v}'$ is the fluctuating constituent of the turbulent flow velocity, $\boldsymbol{R}$ is the curvature radius of $\boldsymbol{v}'$-streamline, $R = |\boldsymbol{R}|$ and the angle brackets denote statistical averaging; $\omega = \nabla \times \boldsymbol{u}/2$; and γ is the shear coefficient of relative rotation affecting medium particles if $\Omega - \omega \neq 0$. Balance condition (2) differs from the corresponding classical equation by an additional term $\frac{1}{2}\nabla \times \sigma$ that describes the effect of antisymmetric stresses.

The projections of (2) to latitudinal and vertical directions read

$$\frac{1}{r} p_{,\vartheta} = -2\omega^0 \rho_0 u \sin\vartheta + \frac{1}{2}\sigma_{\varphi,z} \tag{4}$$

and

$$- p_{,z} - \frac{1}{2r\cos\vartheta}(\sigma_\varphi \cos\vartheta)_{,\vartheta} - 2\rho_0 \omega^0 u \cos\vartheta + \rho g = 0, \tag{5}$$

where r denotes the Earth radius (considered as constant) and, due to $\omega_\varphi = 0$,

$$\sigma_\varphi = 4\gamma\Omega_\varphi. \tag{6}$$

To determine Ω_φ, we consider the projection of the equation for the moment of momentum $\boldsymbol{M} = \left\langle \boldsymbol{v}' \times \boldsymbol{R} \right\rangle$ to the zonal direction. For the discussed flow pattern this projection reads [21–23].

$$-\sigma_\varphi + \rho_0 m_\varphi = 0, \tag{7}$$

where

$$\rho_0 m_\varphi = -4\kappa\Omega_\varphi - g\left\langle \rho' R_\vartheta \right\rangle. \tag{8}$$

The first term on the right side of (8) is caused by the decay of $\boldsymbol{M}$ due to the scattering of the moment of momentum in the cascading process (κ is the coefficient of the cascade scattering). The second term on the right side of (8) describes the moment arising due to baroclinic instability. When writing (7) we neglect the term describing diffusion of $\boldsymbol{M}$ in the medium.

The RAT accounts for the following expression for $\left\langle \rho' R_\vartheta \right\rangle$:

$$\left\langle \rho' R_\vartheta \right\rangle = k_1 \rho_{,z} \Omega_\varphi - k_2 \frac{1}{r}\frac{\partial\rho}{\partial\vartheta}, \tag{9}$$

in which $k_1, k_2 > 0$.

From (7)–(9) we find

$$\Omega_\varphi = \frac{k_2}{k_1 r}\frac{\rho_{,\vartheta}}{b + \rho_{,z}}, \tag{10}$$

where $b = 4(\gamma + \kappa)/k_1 g$. Expression (10) ties the Ω_φ-field with the spatial structure of the density field.

Balance conditions (4), (5), together with expressions (6), (10) and with the assumption that $p_{,z}$ balances the gravity force,

$$p_{,z} = \rho g, \tag{11}$$

constitute a three-parameter model to determine the velocity field $u = u(\vartheta, z)$ and pressure for the prescribed density field $\rho = \rho(\vartheta, z)$.

2.2. The velocity profile

Using (5), (6), and (11), we find for velocity u,

$$u = -\frac{\gamma}{r\rho_0\omega^0 \cos\vartheta}[\Omega_{\varphi,\vartheta} - \Omega_\varphi \tan\vartheta],$$

or, using (9),

$$u = -\frac{a}{\cos\vartheta}\left[\left(\frac{\rho_{,\vartheta}}{b+\rho_{,z}}\right)_{,\vartheta} - \frac{\rho_{,\vartheta}}{b+\rho_{,z}}\tan\vartheta\right], \tag{12}$$

where

$$a = \frac{k_2}{k_1}\frac{\gamma}{\rho_0\omega^0 r^2}.$$

Measuring the density, the depth and u in units $10^{-3}\rho_0$, appropriately chosen reference depth H and aH, respectively, we obtain for (12) the nondimensional expression

$$u = -\frac{1}{\cos\vartheta}\left[\left(\frac{\rho_{,\vartheta}}{c+\rho_{,z}}\right)_{,\vartheta} - \frac{\rho_{,\vartheta}}{c+\rho_{,z}}\tan\vartheta\right], \tag{13}$$

containing only one nondimensional parameter, $c = bH$. It characterizes the summary effect of the depression of Ω_φ due to the antisymmetric shear and scattering of Ω_φ due to the cascading processes. By using (13), the balance condition (4), together with (6) and (10), determines $p_{,\vartheta}$. There is no flow-generating mechanism (e.g. ocean surface slope) but turbulence included into the model here, therefore velocity u as well as $p_{,\vartheta}$ vanish according to (12) and (4) when turbulence is not generated, i.e. if either γ or k_2 equals zero or if the density field is meridionally homogeneous.

2.3. The model set-up with the ocean surface slope included

For the model, accounting for the ocean surface slope, the pressure gradient in (4) is determined as the total pressure gradient, and velocity u, interpreted as the turbulence-generated ageostrophic constituent of the flow velocity, obtains geo-

strophic addend u_{g}. So, as σ_{φ} is determined as proportional to $\rho_{,\vartheta}/(b+\rho_{,z})$, the value of the ageostrophic velocity constituent u increases with increasing $\rho_{,\vartheta}$. The ageostrophic constituent of the motion field vanishes outside frontal regions where the meridional density gradients are absent or weak, as well as in case the turbulent processes are entirely absent. In these regions balance condition (4) reduces to

$$\frac{1}{r}p_{,\vartheta} = -2\omega^0\rho_0 u_{\mathrm{g}}\sin\vartheta, \tag{14}$$

where

$$p_{,\vartheta} = g\left(\int_{\xi}^{z}\rho\,\mathrm{d}z\right)_{,\vartheta} \le 0,$$

which, together with Eq. (11), leads to the thermal wind balance equation.

3. DISCUSSION

3.1. Density data

Isopycnals of the long-term average potential density anomaly σ_{Θ} along the longitude section of 150°W in the latitude interval 30°S to 80°S are shown in Fig. 1. The potential density is calculated according to the international equation of

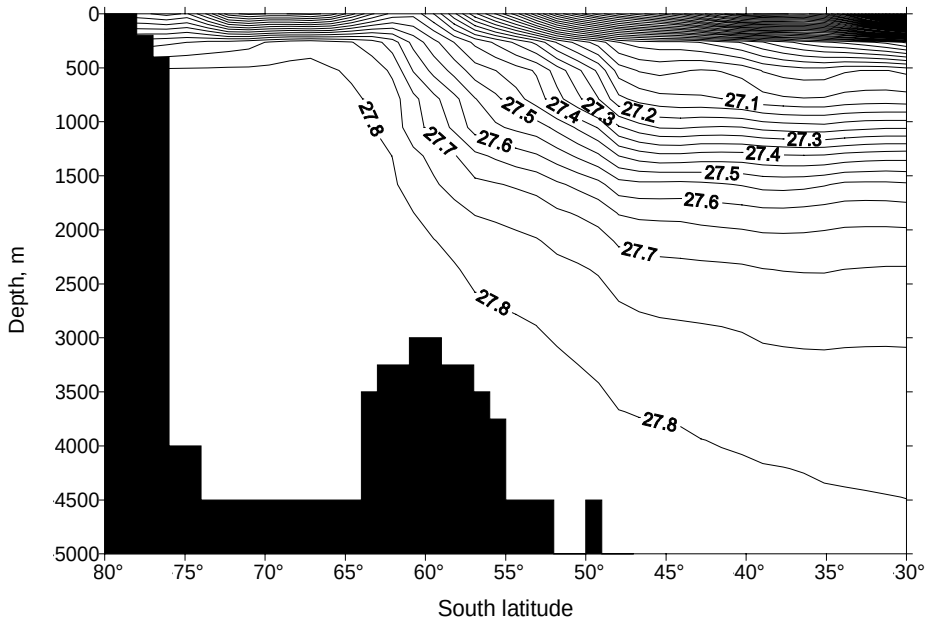

Fig. 1. Distribution of the potential density anomaly σ_{Θ} along longitude 150°W in the Southern Ocean.

state for seawater [30] from optimally analysed Nansen bottle and CTD data on temperature and salinity [31] collected since the 1920s. Two distinct density fronts occur in the section as shown in Figs. 1–3. The southern front, centred at around 57°S, extends deeper, to about 3000 m, while the northern front, located around 37°S, is shallower, being distinguishable down to 350 m.

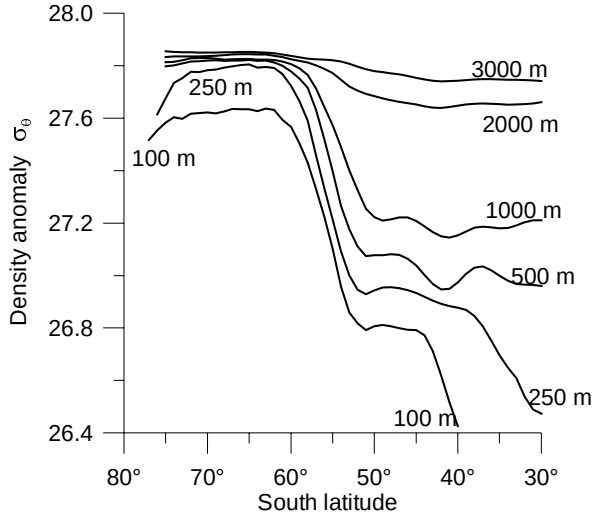

Fig. 2. Horizontal distribution of the potential density anomaly σ_Θ for depths of 100–3000 m along longitude 150°W.

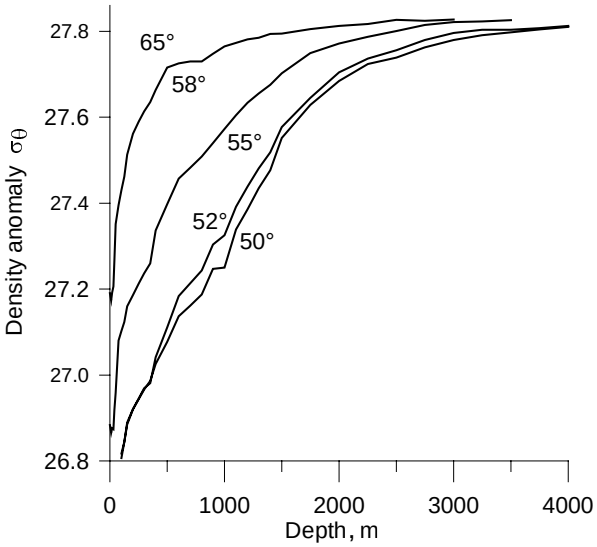

Fig. 3. Vertical distribution of the potential density anomaly σ_Θ for latitudes from 50°S to 65°S along longitude 150°W.

3.2. Calculation of the ageostrophic constituent of flow velocity

Consider the ageostrophic constituent of flow velocity predicted by (13) and calculated for the density field represented in Figs. 1–3. To display the effect of vertical stratification, the velocity calculations were performed for two limit situations.

Figure 4 presents the results of velocity calculation for $c >> \rho_{,z}$. In this case the influence of stratification on the turbulence depression is negligible compared to the effect described by c (see above) and instead of (13) we have

$$cu = -\frac{1}{\cos\vartheta}[\rho_{,\vartheta\vartheta} - \rho_{,\vartheta}\tan\vartheta]. \tag{15}$$

Three resulting ageostrophic current constituents can be clearly distinguished. The centres of the two eastward currents are located at about 55–57°S and at 40–42°S, while the former extends down to 3000 m depth and the latter only to about 350 m depth. The third, westward current to the south of 70°S moves also in the surface layer along the coastal shelf edge. The presented structure of the

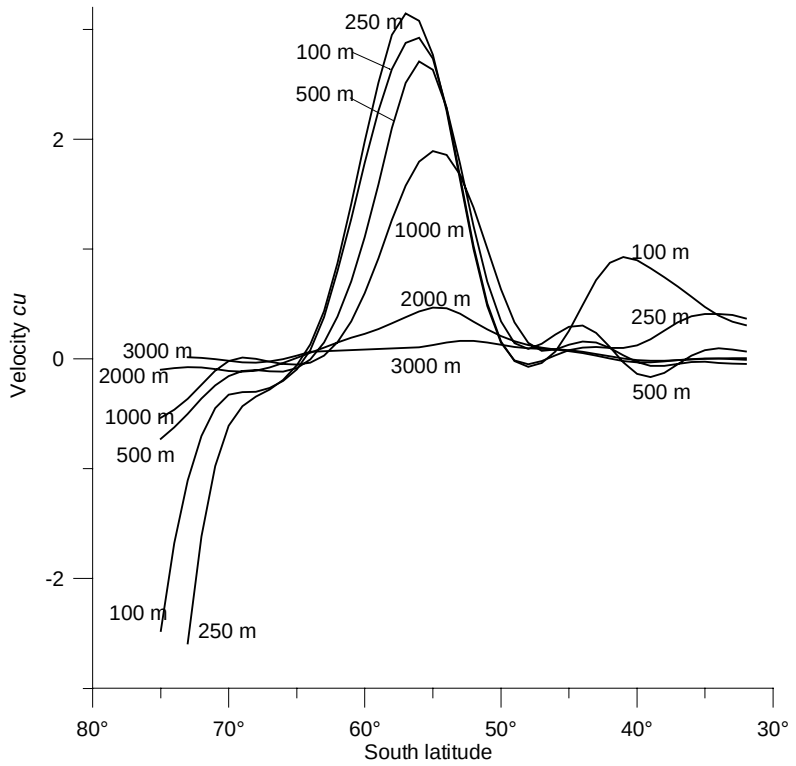

Fig. 4. Ageostrophic velocity profiles along longitude 150°W for depths of 100–3000 m calculated according to (15) ($c >> \rho_{,z}$).

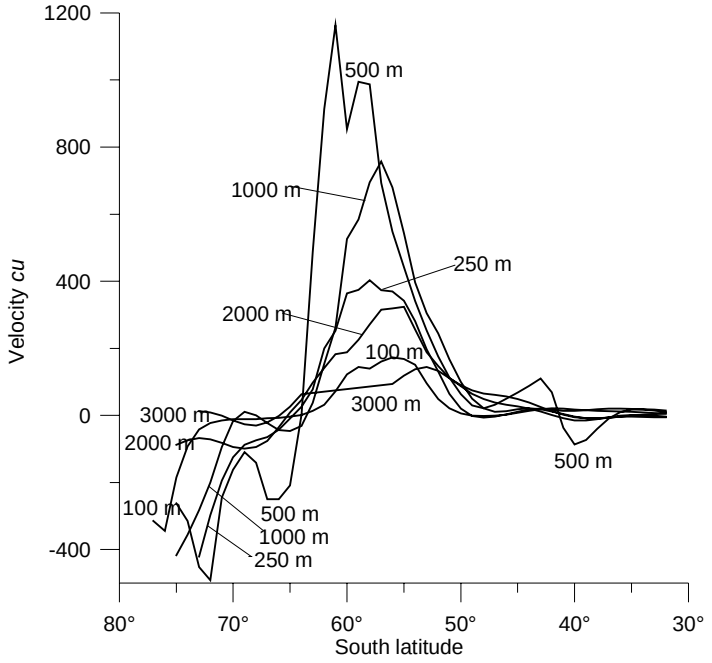

Fig. 5. Ageostrophic velocity profiles along longitude 150°W for depths of 100–3000 m, calculated according to (16) ($c << \rho_{,z}$).

ageostrophic flow velocity mimics the real velocity structure in the Southern Ocean – all three mentioned currents have their counterparts from observations [16]. A long-term (six years) experiment with neutrally buoyant floats at a depth of 900 m, carried out in the South Pacific [26], shows a well-outlined eastward current located at 150°W between 50°S and 60°S. Surface drifting buoy study carried out in 1978–1981 in the Southern Ocean [3] as well as the surface layer (15 m depth) drifter observations of 1978–1999 in the World Ocean [27] confirm the existence of both modelled eastward currents. The westward current along the Antarctic continental slope was investigated by satellite-tracked icebergs in 1972–1977 [27].

Figure 5 presents the results of velocity calculation for $c << \rho_{,z}$. Now formula (14) is simplified to the form

$$u = -\frac{1}{\cos\vartheta}[(\tan\alpha)_{,\vartheta} - \tan\alpha\tan\vartheta], \tag{16}$$

where $\alpha = \alpha(\vartheta, z)$ is the angle between the isopycnal surface $\rho = \text{const.}$ and the horizontal plane $z = \text{const.}$ at (ϑ, z). As can be seen, the strong density stratification to the north of 45°S suppresses here the shallow eastward current.

The velocity calculations performed for the considered limit situations $c >> \rho_{,z}$ and $c << \rho_{,z}$ show the ability of the model to describe (dependent on the value of c) different particular ageostrophic velocity constituent profiles.

4. FORMATION OF THE ACC AGEOSTROPHIC CONSTITUENT IN TERMS OF MASS AND ENERGY BALANCE

4.1. The mass balance

The equation of mass balance is represented as

$$\nabla \cdot \boldsymbol{h} = 0, \tag{17}$$

where

$$\boldsymbol{h} = K \cdot \nabla\rho. \tag{18}$$

In (18) [22,23],

$$K = K^{\mathrm{s}} + K^{\mathrm{as}}, \tag{19}$$

where

$$K^{\mathrm{s}} = (k_0 + k_1\Omega_\varphi^2)\boldsymbol{1}, \qquad K^{\mathrm{as}} = k_2\boldsymbol{E} \cdot \Omega_\varphi \tag{20}$$

($\boldsymbol{E}$ and $\boldsymbol{1}$ are Levi–Civita and unit tensors) determine symmetric and antisymmetric constituents of the turbulent transport tensor K. Taking (19) and (20) into account, the constituents of flux vectors of ρ, associated with the symmetric and antisymmetric constituents of K, are determined as

$$\boldsymbol{h}^{\mathrm{s}} = K^{\mathrm{s}} \cdot \nabla\rho = (k_0 + k_1\Omega_\varphi{}^2)\nabla\rho$$

and

$$\boldsymbol{h}^{\mathrm{as}} = K^{\mathrm{as}} \cdot \nabla\rho = -k_2\Omega_\varphi \times \nabla\rho$$

($\boldsymbol{h} = \boldsymbol{h}^{\mathrm{s}} + \boldsymbol{h}^{\mathrm{as}}$). They describe the fluxes of ρ along the gradient of ρ and perpendicular to it, i.e. along surfaces with constant ρ, respectively.

Using the identity $\nabla \cdot \boldsymbol{h}^{\mathrm{as}} = -\boldsymbol{s} \cdot \nabla\rho$, where $\boldsymbol{s} = k_2\nabla \times \Omega_\varphi$, Eq. (17) can be written as

$$\boldsymbol{s} \cdot \nabla\rho = \nabla \cdot \boldsymbol{h}^{\mathrm{s}}.$$

It shows that the diffusive effect described by $\boldsymbol{h}^{\mathrm{as}}$ mimics the effect of advection caused by the velocity field of incompressible fluid ($\nabla \cdot \boldsymbol{s} = 0$).

So, as $s_\vartheta = k_2\partial\Omega_\varphi/\partial z$, it is easy to conclude that the field $\boldsymbol{s}_\vartheta = s_\vartheta\boldsymbol{i}_\vartheta$, where $\boldsymbol{i}_\vartheta$ is unit vector of coordinate line ϑ, displaces the isopycnals $\rho = \text{const.}$ to the south in layers where Ω_φ increases with depth, and to the north in layers where Ω_φ decreases with depth. This leads to the sloping isopycnals. The slope angle α of isopycnals can be expressed through $\boldsymbol{h}^{\mathrm{as}}$, as $\alpha = \pi/2 - \arccos(\boldsymbol{g} \cdot \boldsymbol{h}_\rho^{\mathrm{as}} / g\,|\boldsymbol{h}_\rho^{\mathrm{as}}|)$ ($\alpha = 0$ for horizontal isolines and $\pi/2$ for vertical isolines). Figure 6 illustrates that situation.

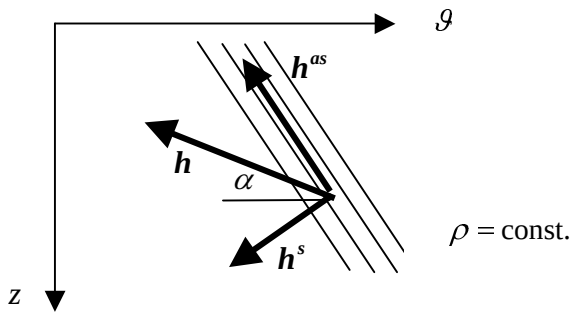

Fig. 6. Scheme of the formation of sloping isopycnals.

4.2. The energy balance

Let us consider now the constructed ACC model in terms of energy balance, accenting interactions between the potential energy $U = -gz\rho$ and the turbulence energy associated with Ω, defined as $K^{\Omega} = J\Omega_{\varphi}^2/2$. Here J denotes the effective moment of inertia, defined from $\boldsymbol{M} = J\Omega$, and residual part of turbulence energy K^0, defined as $K^0 = K^{\mathrm{t}} - K^{\Omega}$, where K^{t} denotes the full turbulence energy defined as $K^{\mathrm{t}} = \langle v'^2 \rangle / 2$.

The equation for the potential energy follows from the equation of mass balance (17) after its multiplication by $-gz$ and is represented as

$$\nabla \cdot (\boldsymbol{h}_U) + Q_0 + Q_1 - Q_2 = 0, \tag{21}$$

where $\boldsymbol{h}_U = -gz\boldsymbol{h}$, $Q_0 = \boldsymbol{h}_0^{\mathrm{s}} \cdot \boldsymbol{g} > 0$, $Q_1 = \boldsymbol{h}_1^{\mathrm{s}} \cdot \boldsymbol{g} > 0$, $Q_2 = -\boldsymbol{h}^{\mathrm{as}} \cdot \boldsymbol{g} > 0$, with $\boldsymbol{h}_0^{\mathrm{s}} = k_0 \nabla\rho$ and $\boldsymbol{h}_1^{\mathrm{s}} = k_1 \Omega_{\varphi}{}^2 \nabla\rho$.

The equation for K^{Ω} balance follows from (6)–(9) and has the form

$$-Q_1 + Q_2 - 4(\gamma + \kappa)\Omega_{\varphi}^2 = 0. \tag{22}$$

If the only sources of energy K^0 are the work described by Q_0 in (21) and $4(\gamma + \kappa)\Omega_{\varphi}^2$ in (22), the energy balance equation for K^0 is expressed as

$$4(\gamma + \kappa)\Omega_{\varphi}^2 - Q_0 - \psi = 0, \tag{23}$$

where $\psi > 0$ denotes the term describing dissipation of energy K^0. From (21)–(23) it follows that

$$\nabla \cdot (\boldsymbol{h}_U) = -\boldsymbol{h} \cdot \boldsymbol{g} = \psi > 0,$$

showing that the situation needs potential energy supply. The energy situation, presented by Eqs. (21)–(23), is illustrated in a graphical form in Fig. 7.

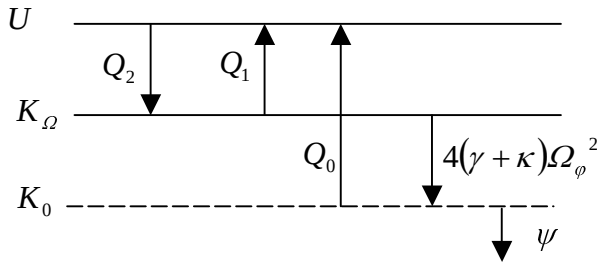

Fig. 7. Scheme of energy interactions.

Let us stress that the described energy balance situation does not include the energy of the average flow. All energy interaction processes leading to the zonal flow formation realize between the energies U, K^{Ω}, and K^{0} only.

5. **CONCLUSIONS**

The discussed model points to the potential importance of turbulent effects in the ACC genesis and, in particular, to the possibility that turbulent processes take full responsibility for the ACC formation. It complements the list of the ACC generating factors (westerlies and geostrophy) with the turbulence fed by the medium potential energy in the density frontal zones. The model does not consider the problems of the origination and persistence of the density field itself, neither does it account for the influence of wind on the ACC. However, the wind friction can be easily included into the description.

It is not known what could be the relative importance of various particular factors influencing the ACC. Most likely the persistent westerlies in the region of the ACC cannot be completely ruled out in the ACC calculations. Nevertheless, considering the wind as the only forcing of the ACC would set the ACC out of the other zonal flow patterns (zonal flows in the Earth's atmosphere as well as in atmospheres of giant planets) which have no analogous forcing. The geostrophic balance could be considered as a common driving mechanism of all zonal flows including the ACC. Though, the geostrophic balance treats the medium as inviscid while the large-scale ocean and atmospheric motions are generally recognized to be turbulent. Furthermore, as it was pointed out in this paper, the turbulence itself can force zonal flows. The problem about the relative importance of different zonal flow formation factors cannot be solved *a priori*. The final solution should come through additional observational evidence.

ACKNOWLEDGEMENTS

The authors thank the anonymous referees for their critical comments. This work was supported by the Estonian Science Foundation (grants Nos. 4781 and 5009/10).

REFERENCES

1. Withworth, T., III, Nowlin, W. D., Jr and Worley, S. J. The net transport of the Antarctic Circumpolar Current through Drake Passage. *J. Phys. Oceanogr*., 1982, **12**, 960–971.
2. Nowlin, W. D., Jr and Klinck, J. M. The physics of the Antarctic Circumpolar Current. *Rev. Geophys.*, 1986, **24**, 469–491.
3. Hofmann, E. E. The large-scale horizontal structure of the Antarctic Circumpolar Current from FGGE drifters. *J. Geophys. Res*., 1985, **90**, 7087–7097.
4. Phillips, H. E. and Rintoul, S. R. Eddy variability and energetics from direct current measurements in the Antarctic Circumpolar Current south of Australia. *J. Phys. Oceanogr*., 2000, **30**, 3050–3076.
5. Rojas, R. Y., Guerrero, Y., Calvete, T. and Garcia, W. WHP repeated hydrography section SR1, Drake Passage. *Int. WOCE Newsl*., 1998, **32**, 38–40.
6. Arhan, M., Garbato, A. C. N., Heywood, K. J. and Stevens, D. P. The Antarctic Circumpolar Current between the Falkland islands and South Georgia. *J. Phys. Oceanogr*., 2002, **32**, 1914–1931.
7. Munk, W. H. and Palmén, E. Note on the dynamics of the Antarctic Circumpolar Current. *Tellus*, 1951, **3**, 53–56.
8. Morrow, R., Church, J., Coleman, R., Chelton, D. and White, N. Eddy momentum flux and its contribution to the Southern Ocean momentum balance. *Nature*, 1992, **357**, 482–484.
9. Johnson, G. C. and Bryden, H. L. On the size of the Antarctic Circumpolar Current. *Deep-Sea Res*., 1989, **36**, 39–53.
10. Gille, S. T. The Southern Ocean momentum balance: evidence for topographic effects from numerical model output and altimeter data. *J. Phys. Oceanogr*., 1997, **27**, 2219–2232.
11. Tansley, C. E. and Marshall, D. P. On the dynamics of wind-driven circumpolar currents. *J. Phys. Oceanogr*., 2001, **31**, 3258–3273.
12. Baker, D. J. A note on Sverdrup balance in the Southern Ocean. *J. Mar. Res.*, 1982, **40**, suppl. 21–26.
13. Hellerman, S. and Rosenstein, M. Normal monthly wind stress over the World Ocean with error estimates. *J. Phys. Oceanogr*., 1983, **13**, 1093–1104.
14. Mestaz-Nunez, A. M., Chelton, D. B. and DeSzoeke, R. A. Evidence of time-dependent Sverdrup circulation in the South Pacific from the Seasat scatterometer and altimeter. *J. Phys. Oceanogr*., 1992, **22**, 934–943.
15. Wyrtki, K. The Antarctic Circumpolar Current and the Antarctic Polar Front. *Dtsch. Hydrogr. Z*., 1960, 13, 153–174.
16. Rintoul, S. R., Hughes, C. W. and Olbers, D. The Antarctic Circumpolar Current System. In *Ocean Circulation and Climate: Observing and Modeling the Global Ocean* (Siedler, G., Church, J. and Gould, J., eds.). *Int. Geophys. Ser*., 2001, **77**, 271–301.
17. Warren, B., LaCasce, J. and Robbins, P. A. On the obscurantist physics of "form drag" in theorizing about the Circumpolar Current. *J. Phys. Oceanogr*., 1996, **26**, 2297–2301.
18. Gnanadesikan, A. and Hallberg, R. W. On the relationship of the Circumpolar Current to Southern Hemisphere winds in coarse-resolution ocean models. *J. Phys. Oceanogr*., 2000, **30**, 2013–2034.
19. Olbers, D. Comments on "On the obscurantist physics of 'form drag' in theorizing about the Circumpolar Current". *J. Phys. Oceanogr*., 1998, **28**, 1647–1654.
20. Karsten, R., Jones, H. and Marshall, J. The role of eddy transfer in setting the stratification and transport of a circumpolar current. *J. Phys. Oceanogr.*, 2002, **32**, 39–54.
21. Heinloo, J. *Phenomenological Mechanics of Turbulent Flows*. Valgus, Tallinn, 1984 (in Russian).
22. Heinloo, J. *Turbulence Mechanics. Introduction to the General Theory of Turbulence*. Estonian Academy of Sciences, Tallinn, 1999 (in Russian).
23. Heinloo, J. Formulation of turbulence mechanics. *Phys. Rev. E*, 2004, **69**, 056317.
24. Aubert, J., Sunghwan, J. S. and Winney, H. L. Observation of zonal flow created by potential vorticity mixing in a rotating fluid. *Geophys. Res. Lett.*, 2002, **29**, 1–14.

25. Christensen, U. R. Zonal flow driven by deep convection in major planets, *Geophys. Res. Lett.*, 2001, **13**, 2553–2556.
26. Davis, R. E. Preliminary results from directly measuring middepth circulation in the tropical and South Pacific. *J. Geophys. Res.*, 1998, **103**(C11), 24619–24639.
27. Niiler, P. The World Ocean surface circulation. In *Ocean Circulation and Climate: Observing and Modelling the Global Ocean*. Academic Press, San Diego, CA, 2001, 193–204.
28. Tchernia, P. and Jeannin, P. F. Observations on the Antarctic East Wind Drift using tabular icebergs tracked by satellite Nimbus F (1975–1977). *Deep-Sea Res.*, 1980, **27**, 467–474.
29. Pedlosky, J. *Geophysical Fluid Dynamics*. Springer-Verlag, New York, 1982.
30. Fofonoff, N. P. and Millard, R. C., Jr. Algorithms for computation of fundamental properties of seawater. *UNESCO Techn. Pap. Marine Sci.*, 1983, **44**.
31. Olbers, D., Gouretski, V., Seiss, G. and Schroeter, J. *Hydrographic Atlas of the Southern Ocean*. Alfred-Wegener-Institut fuer Polar- und Meeresforschung, Bremerhaven, 1992.

Antarktika ringhoovus kui tihedusväljast tingitud voolamine

Jaak Heinloo ja Aleksander Toompuu

Artikkel käsitleb Antarktika ringhoovust kui Lõunaookeani tihedusvälja eripärast tulenevat nähtust. Erinevalt geostroofilisel balansil põhinevast analoogsest käsitlusest võtab formuleeritav käsitlus arvesse liikumise turbulentset iseloomu ning keskkonnas genereeritava turbulentsi pöördelist mitteisotroopsust. Käsitluse formuleerimisel lähtutakse pöördeliselt mitteisotroopsete turbulentsete keskkondade mehaanikast (PMT-teooriast). Lähtudes Lõunaookeanis pika aja vältel mõõdetud ja optimaalanalüüsiga interpoleeritud temperatuuri ja soolsuse väljade alusel hinnatud tihedusvälja struktuurist, näidatakse, et liikumise turbulentne iseloom võib genereerida itta suunatud tsonaalse hoovuse ageostroofilise komponendi. Nimetatud hoovuse komponenti ei esine, kui keskkonnas turbulents puudub. Formuleeritud mudel taandub sellisel juhul klassikalisele käsitlusele geostroofilise balansi raames.